

OccFiner: Offboard Occupancy Refinement with Hybrid Propagation

Hao Shi^{1,5,*}, Song Wang^{1,*}, Jiaming Zhang³, Xiaoting Yin¹, Zhongdao Wang⁴,
 Zhijian Zhao⁵, Guangming Wang⁶, Jianke Zhu¹,
 Kailun Yang^{2,†}, and Kaiwei Wang^{1,†}

¹Zhejiang University, ²Hunan University, ³Karlsruhe Institute of Technology,
⁴Huawei Noah's Ark Lab, ⁵Supremind, ⁶University of Cambridge

Abstract. Vision-based occupancy prediction, also known as 3D Semantic Scene Completion (SSC), presents a significant challenge in computer vision. Previous methods, confined to onboard processing, struggle with simultaneous geometric and semantic estimation, continuity across varying viewpoints, and single-view occlusion. Our paper introduces OccFiner, a novel *offboard* framework designed to enhance the accuracy of vision-based occupancy predictions. OccFiner operates in two hybrid phases: 1) a *multi-to-multi local propagation network* that implicitly aligns and processes multiple local frames for correcting onboard model errors and consistently enhancing occupancy accuracy across all distances. 2) the *region-centric global propagation*, focuses on refining labels using explicit multi-view geometry and integrating sensor bias, especially to increase the accuracy of distant occupied voxels. Extensive experiments demonstrate that OccFiner improves both geometric and semantic accuracy across various types of coarse occupancy, setting a new state-of-the-art performance on the SemanticKITTI dataset. Notably, OccFiner elevates vision-based SSC models to a level even surpassing that of LiDAR-based onboard SSC models.

Keywords: Semantic Scene Completion · 3D Occupancy Prediction · Offboard Perception

1 Introduction

Vision-based Occupancy Prediction, often referred to as Semantic Scene Completion (SSC), is a process aimed at accurately reconstructing the geometry and semantics of a surrounding 3D scene from the image captures [6]. Compared to LiDAR solutions, camera-based systems offer the benefits of being lightweight, cost-effective, and ease of deployment and maintenance. Most SSC efforts are made in onboard settings [6, 27, 52], *i.e.*, data calculation and feedback take place on the mounted vehicle. However, integrating data into offboard systems

* Equal contribution

† Correspondence: kailun.yang@hnu.edu.cn, wangkaiwei@zju.edu.cn

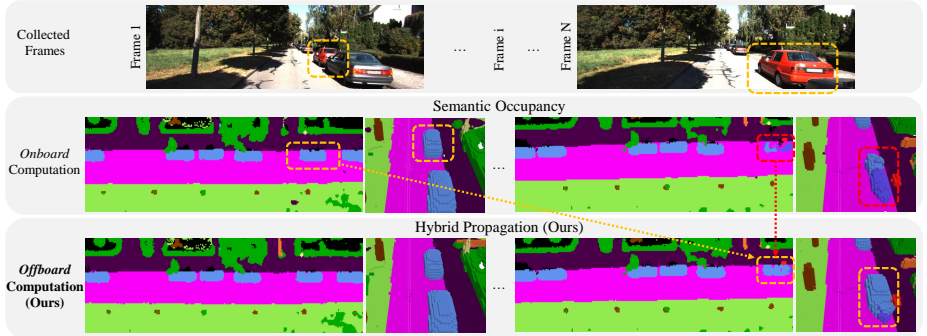


Fig. 1: Current *onboard* methods generate unreliable occupancy predictions that are inconsistent across different viewpoints. In contrast, our *offboard* framework constructs a unified and multi-view consistent occupancy map with higher accuracy.

creates opportunities for identifying and rectifying potential deficiencies in models. Consequently, we propose offboard SSC, a new setup that entails additional computation and refinement of on-vehicle predictions at a data center. It can play a pivotal role in auto-labeling by leveraging aggregated and diverse data from multiple sources, significantly reducing manual annotation efforts and improving labeling accuracy for large-scale 3D scene understanding [24, 25, 77].

Despite various research efforts [6, 18, 27], vision-based SSC has fallen short in accuracy compared to LiDAR solutions. There are two limitations: 1) The depth measurement of monocular cameras lacks the precision of LiDAR systems, requiring onboard vision-based SSC methods to struggle with both geometry and semantics. 2) Onboard models are limited to processing a restricted number of local frames, impacting accuracy and multi-view continuity in both vision- and LiDAR-based SSC. This issue manifests as unreliable estimations and discontinuities across viewpoints in geometry and semantics, as illustrated in Fig. 1. We argue that high-fidelity SSC maps should remain consistent across viewpoints to ensure safety and reliability, especially since static rigid objects should not exhibit significant changes in classes. While offboard systems offer refined evaluation of onboard model performance, essential for the data closed-loop in autonomous driving [24, 25, 77], their potential in SSC remains under-explored.

Given such limitations of inferior performance and onboard SSC setting, we introduce **OccFiner**, the first *offboard* occupancy refinement framework. The objective is to significantly enhance the reliability of vision-based SSC. By doing so, the constructed 3D SSC map can be reliably used repeatedly after a one-time low-cost acquisition with only cameras. Specifically, we consider two primary error sources in addressing the inaccuracies of vision-based SSC: the prediction bias error introduced by the onboard model, and the measurement bias from the camera capture process. OccFiner decouples these two heterogeneous error sources and uses a two-stage hybrid process to process them separately: (1) *Multi-to-Multi Local Propagation*. In the initial stage, OccFiner addresses prediction bias errors from the onboard model. We implement an error com-

pensation model that processes inputs from off-the-shelf SSC models [6, 27, 52]. This model uniquely encodes relative spatial coordinates within a local window, facilitating the propagation of geometric and semantic cues by a newly proposed DualFlow4D transformer. This approach effectively enhances the accuracy of occupancy predictions at varying distances. (2) *Region-centric Global Propagation*. The second stage focuses on measurement errors from camera captures. Here, OccFiner employs explicit multi-view geometry to register and aggregate data across the entire scene, incorporating sensor bias weighting in the process. Compared with the simple accumulation of multi-frame averages, our region-centric voting strategy yields a more accurate SSC map. By integrating local implicit error compensation and non-local explicit information propagation from various viewpoints, OccFiner effectively addresses onboard bias, multi-view consistency, and single-view occlusions, therefore naturally enhancing the reliability and robustness of scene understanding.

To the best of our knowledge, we are the first to introduce offboard refinement for SSC. Our method, termed OccFiner, enables seamless integration across various SSC models and datasets as a plug-and-play solution. For 3D semantic scene completion on SemanticKITTI dataset [2], OccFiner has demonstrated remarkable performance, surpassing VoxFormer by 3.67% in mIoU, which makes a 26.99% relative improvement and ranks first on the test leaderboard among all monocular methods. Surprisingly, OccRefiner also works well for LiDAR-based SSC [65] with minor changes, leading to a new state-of-the-art of 37.82% in mIoU, achieving a 9.5% improvement compared with the best benchmark result.

To summarize, we deliver the following contributions:

- We are the first to explore the problem of learning to generate high-quality vision-oriented SSC maps offboard.
- We propose OccFiner, an effective offboard occupancy refinement framework with hybrid propagation to build multi-view consistent SSC maps.
- OccFiner sets new state-of-the-art performances in both camera-based and LiDAR-based SSC. For the first time, the accuracy of the camera-based SSC method surpasses that of the classical onboard LiDAR-based method [55].

2 Related Work

2.1 3D Semantic Scene Completion

Semantic Scene Completion (SSC), also known as Semantic Occupancy Prediction, aims at concurrently estimating the geometry and semantics of a surrounding scene. The first effort SSCNet [55] lays the foundation for this field by defining the SSC task and introducing a method for estimating the structure and semantics of indoor scenes from a singular depth image input. Recognizing the critical role of SSC-based perception in the realm of autonomous driving, researchers have increasingly turned their attention to its applications in outdoor scenes after the release of the large-scale outdoor benchmark SemanticKITTI [2]. The predominant works in this area can be broadly categorized based on the

input modality: LiDAR-based SSC [8, 51, 52, 65, 69, 70, 73, 85] and vision-based SSC [6, 16, 20, 29, 33–36, 38, 53, 63, 64, 75, 82]. Additionally, recent research expands into several novel areas within SSC including the world model [83], 3D object detection [15, 19, 41, 49, 59, 68, 84], multimodal parsing [22, 31, 39, 42, 43, 45, 66, 74, 79], self-supervised prediction [4, 14, 17, 40, 78], open-vocabulary recognition [57, 60], dense top-view understanding [12, 32, 48], V2X collaboration [28, 54, 81], as well as various benchmarks [26, 58, 62]. However, the majority of previous studies have concentrated on methodological design within onboard settings, where observations across different viewpoints often exhibit notable discontinuities. In contrast, OccFiner shifts focus to the offboard setting, aiming to rectify errors inherent in onboard models and to aggregate long-term geometric and semantic cues. Our approach contributes to data closure in autonomous driving, addressing a crucial aspect that has been largely overlooked in previous SSC research.

2.2 Offboard 3D Perception

Perception in autonomous driving scenarios necessitates extensive data annotation and training [5, 11, 56]. Since LiDAR can provide accurate range information in 3D space, researchers explore its sequence learning in semantic segmentation [1, 61], object detection [44, 47] and tracking [46] to obtain better performance. The sequential characteristics of LiDAR scans are further studied in offboard 3D object detection [10, 37, 50, 71] to reduce annotation costs. 3DAL [50] formulates the problem of offboard 3D object detection and proposes an *object-centric* auto-labeling detector. CTRL [10] adheres to the principle of *track-centric* and elevates the accuracy of auto-labeling, surpassing manual annotation in some scenarios. The aforementioned methods are all designed for LiDAR point cloud, attributed to the ease of accumulating 3D spatial information compared to images. MV-Map [67] provides a *region-centric* fusion solution for high-definition maps with camera data as inputs while it only processes limited traffic elements on the bird’s eye view plane. To address the above challenges, We design the first hybrid propagation pipeline (OccFiner) for offboard semantic scene completion (SSC). OccFiner can process the SSC predictions from either cameras or LiDAR and provide high-quality occupancy information for autonomous vehicles, which holds significant importance in auto-labeling and data closure in pure visual perception.

3 Approach

3.1 Overview

The OccFiner framework, designed for offboard Semantic Scene Completion (SSC), operates in two distinct stages. The first stage focuses on compensating for errors in onboard model predictions, employing a multi-to-multi local propagation network to process SSC model outputs across a series of frames, utilizing both close-range and distant frames as references. This stage effectively merges

relative spatial coordinates with semantic features, employing transformer-based methods for spatio-temporal integration. The second stage of OccFiner emphasizes global semantic and geometric aggregation. It transforms refined voxel labels into semantic point clouds and applies relative poses over extended periods for precise coordinate adjustments, incorporating sensor measurement characteristics for voxel voting. This dual-stage strategy effectively combines local implicit feature propagation with global explicit semantic aggregation, forming a robust hybrid system for offboard SSC refinement.

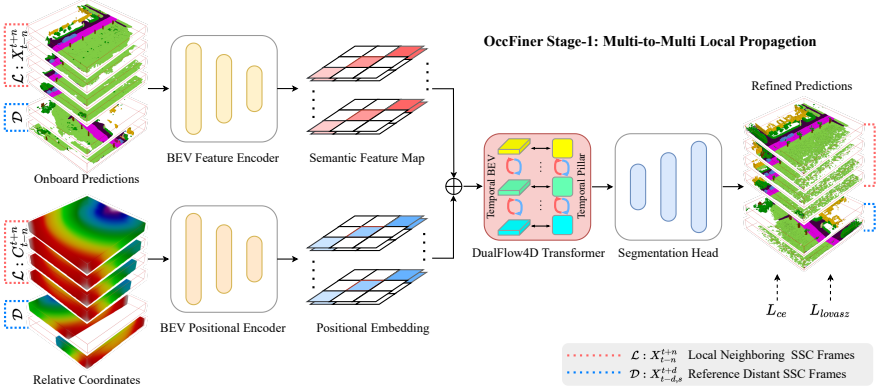


Fig. 2: Overview of the proposed multi-to-multi local propagation network. It accepts multiple onboard predictions and relative coordinates as input. This network adeptly executes error compensation and facilitates the implicit local propagation, improving SSC quality across various distances.

3.2 Multi-to-Multi Local Propagation Network

Problem formulation: Let $X_1^T := \{X_1, X_2, \dots, X_T\}$ be a onboard SSC inference sequence of height H , width W , depth Z , and frames length T . $C_1^T := \{C_1, C_2, \dots, C_T\}$ denotes the corresponding frame-wise relative coordinates, which can be calculated by:

$$\mathbf{c}_i = (T_{li}^{cam})^\top (T_{cam_t}^{world})^\top T_{cam_i}^{world} T_{li}^{cam} \mathbf{x}_i, \quad (1)$$

where each vertex $\mathbf{x}_i \in X_i$ is projectively associated to a relative vertex $\mathbf{c}_i \in C_i$. For each relative coordinate C_i , it represents the mapping relationship between the three-dimensional coordinates of the current frame X_i and the coordinates of the pivot frame X_t . We formulate the occupancy refinement as a task that takes the onboard (X_1^T, C_1^T) pairs as input and reconstruct the SSC labels $Y_1^T = \{Y_1, Y_2, \dots, Y_T\}$. Specifically, we propose to learn a mapping function from onboard inferences X_1^T to the output $\hat{Y}_1^T := \{\hat{Y}_1, \hat{Y}_2, \dots, \hat{Y}_T\}$, such that the conditional distribution of the real data $p(Y_1^T | X_1^T)$ can be approximated by the one of generated data $p(\hat{Y}_1^T | X_1^T)$.

We conceptualize the task as a “multi-to-multi” prediction problem, focusing on the simultaneous refinement of all input SSC frames in a single feed-forward

process. The intuition is that regions obscured in the current viewpoint are likely to become visible in frames captured from a distance, particularly in scenarios involving large occlusions or when the vehicle is moving at a slower pace. In the context of multi-frame offboard SSC, it is more effective to address gaps in a target frame by leveraging content from the entire scene sequence, incorporating information from both neighboring and distant frames as conditional inputs. This approach relies on the Markov assumption [13] for simplification, which allows us to express the refinement process as:

$$p(\hat{Y}_1^T | X_1^T) = \prod_{t=1}^T p(\hat{Y}_{t-n}^{t+n} | X_{t-n}^{t+n}, X_{t-d,s}^{t+d}), \quad (2)$$

where X_{t-n}^{t+n} represents a short SSC clip of neighboring frames centered around time t with a temporal radius n . $X_{t-d,s}^{t+d}$ denotes distant frames that are randomly sampled from a distant scene range d at a rate of s . This selection of distant frames typically encompasses most of the key moments in possible viewpoints, effectively conveying long-term geometric and semantic cues of the scene.

Within this framework, offboard SSC models are tasked with not only maintaining temporal consistency in neighboring frames but also ensuring that the refined frames are coherent with the broader narrative of the scene sequence. This approach aims to enhance scene understanding by integrating both local and global temporal perspectives in the refinement process.

Network design: The overview of the proposed multi-to-multi local propagation network is shown in Fig. 2. As indicated in Eq. 2, OccFiner takes both neighboring local SSC frames X_{t-n}^{t+n} , distant reference SSC frames $X_{t-d,s}^{t+d}$, and relative coordinate $\{C_{t-n}^{t+n}, C_{t-d,s}^{t+d}\}$ as conditions, to propagate across all input frames simultaneously. Specifically, OccFiner is comprised of four integral components, including a frame-level BEV feature encoder, a parallel BEV positional encoder, a series of spatial-temporal transformers, and a frame-level segmentation head. The frame-level BEV feature encoder is architecturally configured with multiple 2D convolutions along the horizontal and vertical dimensions (X, Y), thus converting the height dimension (Z) into a feature dimension. Mirroring this, the frame-level BEV positional encoder shares the same architectural blueprint with the feature encoder, such a design choice aids in better aligning the positional and feature information, as both are processed through a similar computational pathway. At the heart of OccFiner lie the DualFlow4D transformers, tasked with learning and applying joint spatial-temporal transformations. These transformers are specifically tailored to address uncertainties and occlusions within the deep encoding space.

DualFlow4D transformer: To propagate high-fidelity features in each SSC frame, multi-layer DualFlow4D transformers are designed to search coherent contents from all the encoded features. Specifically, we propose to first search by a multi-head soft-patch-based focal attention module along BEV and temporal dimensions. We use $f_1^T = \{f_1, f_2, \dots, f_T\}$, where $f_i \in \mathbb{R}^{h \times w \times c}$ to denote the features encoded from the frame-level BEV encoder. Concurrently, $p_l \in \mathbb{R}^{T_l \times h \times w \times c}$ and $p_r \in \mathbb{R}^{T_r \times h \times w \times c}$ encapsulate the corresponding encoded local and refer-

ence relative coordinates. We first use soft split to embed them into overlapped patches $P \in \mathbb{R}^{(T_l+T_r) \times W_h \times W_w \times c_e}$:

$$P = \text{SS}((f_l \oplus f_r) + (p_l \oplus p_r)), \quad (3)$$

where $\text{SS}(\cdot)$ denotes the soft split operation, which softly splits each BEV feature into overlapped patches of size $W_h \times W_w \times T$ with stride k , and flattened to a one-dimensional token, which is similar to the image splitting strategy in T2T-ViT [76]. T_l and T_r are the time dimension of local frames and reference frames, and W_h and W_w are the spatial dimension of embedded tokens. \oplus denotes the feature concatenation. The overlapped position aggregates a piece of information from different tokens, contributing to smoother semantic patch boundaries and enlarging its receptive field by fusing cues from neighboring patches.

Instead of the vanilla vision transformer [9], we use focal transformer [72] to search from both local and non-local neighbors to propagate high-fidelity BEV features. Concretely, P is linearly projected to queries Q , keys K , and values V for computing the 3D focal attention:

$$\begin{aligned} Q, K, V &= \mathcal{P}_{qkv}(\text{LN}(P)), \\ Z_{bev} &= \text{MHFA}(Q, K, V) + P, \end{aligned} \quad (4)$$

where LN and MHFA denote the layer normalization and multi-head focal attention, respectively, \mathcal{P}_{qkv} is the linear projection layer. We omit the time dimension for simplicity. The previous propagation is limited to the temporal BEV space. To ensure effective propagation in the height direction, we have additionally introduced attention along the z-axis, specifically focusing on the ‘pillar’, which refers to a voxel grid oriented along the height:

$$Z_z := \text{Attn}(Q_z, K_z, V_z) = \text{Softmax}\left(\frac{Q_z K_z^\top V_z}{\sqrt{d}}\right), \quad (5)$$

where $Q_z, K_z, V_z \in \mathbb{R}^{W_z \times T \times c_e}$ are respectively reshaped queries, keys, and values. Finally, the output of the entire propagated feature will be gathered:

$$Z_{4d} = \mathcal{P}_z(Z_z) + \mathcal{P}_{bev}(Z_{bev}), \quad (6)$$

where \mathcal{P}_z and \mathcal{P}_{bev} are linear projections. Note that the above formulas omit the head dimension for simplicity. Such a 4D dual-branch design promotes learning coherent spatial-temporal transformations by preserving both BEV information flow and the height dimension information flow along the pillar-shape voxels.

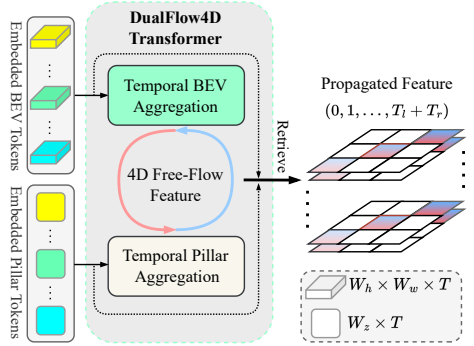


Fig. 3: Our proposed DualFlow4D transformer block. It engages spatiotemporal propagation within BEV space and vanilla attention to pillar tokens. This dual approach enables effective matching and flow of semantic and geometric cues for comprehensive scene understanding.

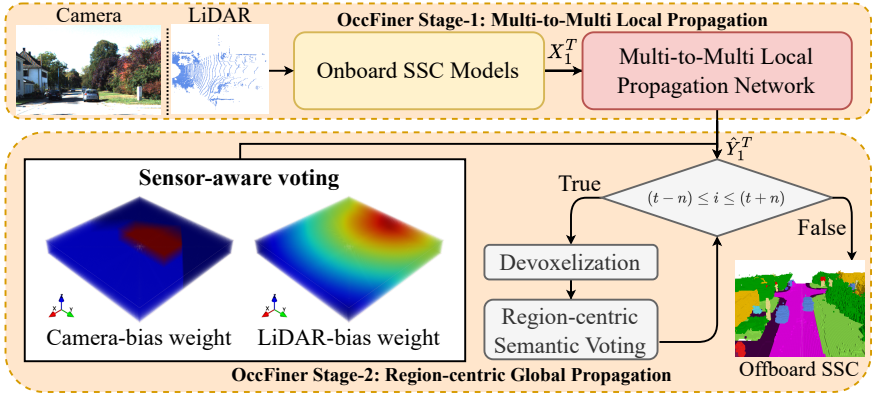


Fig. 4: Overview of the proposed region-centric global propagation. Given an arbitrary number of input frames, we leverage multi-view geometry and consider sensor bias to augment long-term SSC consistency and accuracy.

3.3 Region-centric Global Propagation

In the initial stage, the OccFiner framework engages in multi-to-multi local propagation for offboard SSC (Semantic Scene Completion) refinement. This stage, however, is limited by the input multi-frame window size, leading to a necessity for global propagation across the entire scene sequence. Notably, the local propagation process uniformly enhances SSC accuracy regardless of the various distances, a key aspect of global propagation’s effectiveness. Additionally, OccFiner utilizes relative coordinates in the initial stage, ensuring the implicit alignment of multiple frames and maintaining the contextual integrity of each frame’s semantic content. This approach, which prevents truncation, is pivotal for learning-based error compensation. The subsequent stage involves geometric explicit registration voting, covering the entire scene sequence, and forming a cohesive and hybrid strategy within the OccFiner framework. In the global propagation stage, OccFiner focuses on addressing the measurement limitations of camera and LiDAR sensors and aggregates the independent SSC predictions into a multi-view consistent prediction for each region. OccFiner adeptly integrates sensor-aware weight biases with vanilla registration methods, aligning the refinement process with the unique attributes of each sensor type. Next, we delve into the details of vanilla registration and enhanced sensor-aware registration.

Vanilla Registration: As illustrated in Fig. 4, it aggregates independent SSC predictions from $2n + 1$ frames into a multi-view consistent prediction for each region, where n is the temporal window radius. This involves the aggregation of per-frame semantics and geometry $\{\hat{Y}_i\}_{i=1}^{2n+1}$ into a refined SSC map. For a given target voxel index \mathbf{y} within a 3D region of target \hat{Y}_{tg} , the process starts with devoxelizing the current SSC voxel \hat{Y}_{cur} to derive the semantic point cloud \mathbf{P}_{cur} in the current LiDAR coordinate system:

$$\mathbf{P}_{cur}(x, y, z, c) = \left\{ (o_x + i \cdot dv_x, o_y + j \cdot dv_y, o_z + k \cdot dv_z, c) \mid \hat{Y}_{ijk} = c \right\}, \quad (7)$$

where the voxel origin is (o_x, o_y, o_z) . dv denotes the voxel size and c represents the semantic classes. This point cloud is then transformed relative to the target LiDAR coordinate system with poses $\{T_{cur}^{tg}\}_{tg=n}^{tg+n}$.

$$\mathbf{P}_{cur}^{tg} = T_{cur}^{tg} \mathbf{P}_{cur}, \quad (8)$$

followed by voxelization and addition in the voting voxel. The final step involves voting for the final semantic voxel output \bar{Y}_{final} :

$$\bar{Y}_{final} = \underset{c}{\operatorname{argmax}} \left(\sum_{cur=tg-n}^{tg+n} \text{Voxelize}(\mathbf{P}_{cur}^{tg}, c) \right), \quad (9)$$

where the argmax function selects the class c with the highest aggregated value in the voting voxel, determining the final semantic voxel.

Incorporating with Sensor Bias: While vanilla registration averages SSC across multiple frames, it overlooks the differential weighting of different locations. To address this, sensor-aware weighting is introduced, tailored to the distinct characteristics of cameras and LiDARs. This approach is informed by the measurement characteristics of measurement devices like cameras and LiDARs. Camera systems are constrained by their field of view, with points within the viewing frustum yielding higher accuracy compared to those outside. Additionally, the occlusion of distant points by nearer ones necessitates lower voting weights for the former. Conversely, LiDAR systems exhibit increased sparsity and depth measurement errors at longer distances. Therefore, for cameras, points within the field of view and at closer ranges are given higher voting weights:

$$F_{cam}(x_c, y_c, z_c) = \left(|\theta_{xc}| \leq \frac{fov_h}{2} \right) \wedge \left(|\theta_{yc}| \leq \frac{fov_w}{2} \right) \wedge (z_c > 0), \quad (10)$$

$$W_{cam}(\mathbf{x}) = \begin{cases} w_{\text{high}}, & \text{if } (F_{cam} \wedge B)(\mathbf{x}) > 0 \\ w_{\text{med}}, & \text{if } [F_{cam}(\mathbf{x}) > 0] \wedge [B(\mathbf{x}) < 0] \\ w_{\text{low}}, & \text{otherwise} \end{cases} \quad (11)$$

where (x_c, y_c, z_c) are the voxel indices in the camera coordinate system, fov denotes the field of view of the camera, F_{cam} represents the voxels within the frustum, and B is the bounding box voxel with values being True inside the box and False outside. \mathbf{x} is the vertex and W_{cam} is the final camera voting weight.

While for LiDARs, the voting weight linearly attenuates with increasing distance from the LiDAR center:

$$W_{li}(r) = w_{\max} - (w_{\max} - w_{\min}) \times \frac{r}{R}, \quad (12)$$

where r denotes the radial distance from the origin in the LiDAR coordinate system, R represents the maximum range, and w_{\max} and w_{\min} correspond to the maximum and minimum weights, respectively. Consequently, the OccFiner framework adopts a hybrid dual-stage strategy: the first stage addresses onboard model errors, enhancing prediction accuracy regardless of the range, and the second stage adjusts for the physical limitations of cameras and LiDARs, further improving the offboard accuracy.

3.4 Supervision

Our multi-to-multi local propagation network is trained with the labels from the training set frame-by-frame, while the region-centric global propagation is a learning-free process. The SSC loss \mathcal{L}_{ssc} for network training consists of two parts as below:

$$\mathcal{L}_{ssc} = \mathcal{L}_{ce} + \mathcal{L}_{lovasz}, \quad (13)$$

where \mathcal{L}_{ce} is the cross-entropy loss and \mathcal{L}_{lovasz} is the Lovász loss [3].

4 Experiments

4.1 Datasets and Implementation Details

SemanticKITTI and SSCBench-KITTI360: The SemanticKITTI dataset [2] is a pivotal SSC benchmark featuring 22 outdoor driving scenarios, segmented into train, validation, and test sets with a 10/1/11 split. The focus is on a specific volume around the vehicle, mapped in $256 \times 256 \times 32$ voxel grids, where each voxel measures $0.2m^3$. SSCBench-KITTI360 [26], derived from KITTI-360 [30], spans $73.7km$ with extensive image and laser scan data, providing diverse geographical coverage and extended sequences. This dataset, sampled to reduce redundancy, offers around $13k$ frames, serving as a vital resource for SSC research.

Training and Optimization: Models are trained for 10 epochs on the SemanticKITTI and 15 on SSCBench-KITTI360, using the Adam optimizer [21] with a learning rate of 0.001. The rate decay is 0.98^{epoch} . Training is performed on 8 RTX 3090 GPUs and includes x-y flipping augmentation in 3D volume space.

4.2 Comparison with State-of-the-Art

As our work presents the *first* offboard SSC generation, there are no existing competitors to parallel OccFiner’s performance. Additionally, our OccFiner can utilize any off-the-shelf onboard model as its intermediate component. As shown in Tab. 1, we use the camera-based SSC algorithm [6, 18, 27] as the onboard component. On the SemanticKITTI validation set [2], OccFiner demonstrates substantial improvements in mIoU accuracy for various algorithms like MonoScene [6], TPVFormer [18], and VoxFormer [27]. The mIoU accuracy is relatively improved by 21.39%, 17.08%, and 35.71%, respectively. Notably, OccFiner (Vox) achieves the new state-of-the-art camera SSC accuracy of 18.09% mIoU. To ensure a meaningful and fair comparison, we also establish an offboard baseline algorithm, “Average Fusion”. It performs region-centric aggregation without learning refinement or considering sensor measurement biases. Despite this, compared to VoxFormer + Average Fusion, our OccFiner (Vox) can still improve SSC quality by a large margin of over 24.59% in mIoU under the long-range setting.

Qualitative comparisons. As shown in Fig. 5, our offboard solution, OccFiner, effectively corrects major onboard errors, notably in resolving extensive missing road and vehicle voxels. Furthermore, OccFiner enhances the effectiveness

Table 1: Camera-based semantic scene completion results on the SemanticKITTI validation set [2]. * represents these methods are adapted for the RGB inputs, which are implemented and reported in MonoScene [6]. † represents the reproduced result from [18].

Method	car (3.02%)	bicycle (0.03%)	motorcycle (0.03%)	truck (0.16%)	other-vehicle (0.20%)	person (0.07%)	bicyclist (0.07%)	motorcyclist (0.03%)	road (15.30%)	parking (1.12%)	sidewalk (11.13%)	other-ground (0.50%)	building (14.1%)	fence (3.30%)	vegetation (39.3%)	trunk (0.15%)	terrain (0.17%)	pole (0.20%)	traffic-sign (0.08%)	IoU	mIoU
LMSCNet* [52]	18.33	0.00	0.00	0.00	0.00	0.00	0.00	0.00	40.68	4.38	18.22	0.00	10.31	1.21	13.66	0.02	20.54	0.00	0.00	28.61	6.70
3DSSketch* [7]	18.59	0.00	0.00	0.00	0.00	0.00	0.00	0.00	41.32	0.00	21.63	0.00	14.81	0.73	19.09	0.00	26.40	0.00	0.00	33.30	7.50
AICNet* [24]	14.71	0.00	0.00	4.53	0.00	0.00	0.00	0.00	43.55	11.97	20.55	0.07	12.94	2.52	15.37	2.90	28.71	0.06	0.00	29.59	8.31
JSCNet* [70]	24.65	0.00	0.00	4.41	6.15	0.67	0.27	0.00	50.49	11.94	23.74	0.07	15.03	3.94	18.11	4.33	26.86	3.77	1.45	38.98	10.31
OccFormer [82]	25.09	0.81	1.19	25.53	8.52	2.78	2.82	0.00	58.85	19.61	26.88	0.31	14.40	5.61	19.63	3.93	32.62	4.26	2.86	36.50	13.46
MonoScene† [6]	23.26	0.61	0.45	6.98	1.48	1.86	1.20	0.00	56.52	14.27	26.72	0.46	14.09	5.84	17.89	2.81	29.64	4.14	2.25	36.86	11.08
TPVFormer [18]	23.81	0.36	0.05	8.08	4.35	0.51	0.89	0.00	56.50	20.60	25.87	0.85	13.88	5.94	16.92	2.26	30.38	3.14	1.52	35.61	11.36
VoxFormer [27]	27.01	1.05	0.47	9.90	4.64	1.51	0.85	0.00	54.67	18.55	27.35	0.41	19.65	8.52	26.18	6.58	32.39	8.69	4.71	44.16	13.33
Average Fusion (Vox)	30.35	0.88	0.41	12.92	3.99	1.60	0.86	0.00	57.60	18.53	29.44	0.28	21.83	10.50	29.24	7.44	34.61	9.79	5.54	46.03	14.52
OccFiner (Mono)	29.12	0.41	1.41	21.19	7.85	3.97	2.28	0.00	56.62	19.64	27.62	1.48	15.07	7.18	20.89	3.89	31.79	3.92	2.39	37.42	13.45
w.r.t. MonoScene	+5.86	-0.20	+0.96	+14.21	+6.37	+2.11	+1.08	-	+0.10	+5.37	+0.90	+1.02	+0.98	+1.34	+3.00	+1.08	+2.15	-0.22	+0.14	+5.06	+2.37
OccFiner (TPV)	29.19	0.69	0.00	22.73	7.05	0.95	1.40	0.00	57.15	22.78	28.35	7.93	15.10	6.87	19.88	3.09	31.02	3.70	1.92	36.54	13.30
w.r.t. TPVFormer	+5.38	+0.33	-0.05	+14.65	+2.70	+0.44	+0.51	-	+0.65	+2.18	+2.48	+7.08	+1.22	+0.93	+2.96	+0.83	+0.64	+0.56	+0.40	+0.93	+1.94
OccFiner (Vox)	36.78	1.73	0.29	32.96	5.67	4.06	1.12	0.00	66.34	27.05	35.06	0.35	25.46	11.79	32.82	9.87	40.56	8.02	3.58	47.86	18.09
w.r.t. VoxFormer	+9.77	+0.68	-0.18	+22.05	+1.03	+2.55	+0.27	-	+11.67	+8.50	+7.71	-0.06	+5.81	+3.27	+6.64	+3.29	+8.17	-0.67	-1.13	+3.70	+4.76

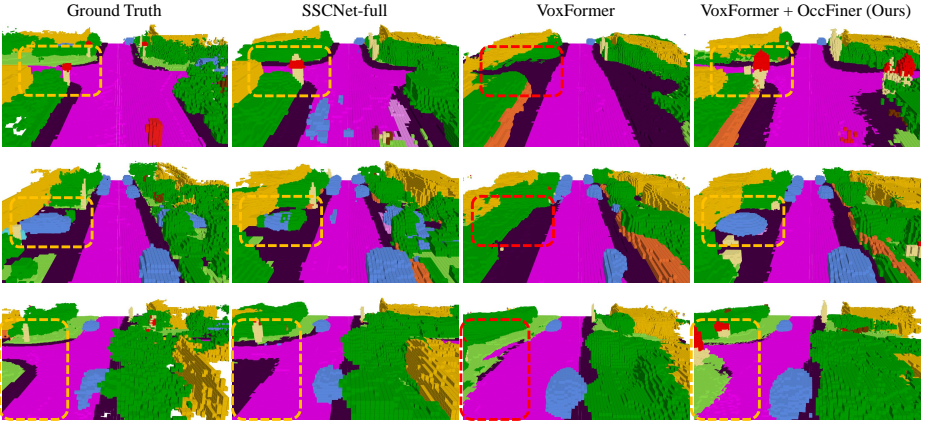


Fig. 5: Qualitative comparisons. Our offboard solution effectively fixes critical errors in onboard component [27], such as large areas of *missing road and vehicles*. Moreover, OccFiner elevates the performance of pure visual solutions beyond the classic *LiDAR-based* onboard method SSCNet-full [55].

of purely visual approaches, surpassing the traditional *LiDAR-based* onboard method SSCNet-full [55] in performance, indicating its potential to advance the field of autonomous navigation with pure visual solution.

Our exploration extends to validating OccFiner’s versatility across different modalities in offboard SSC generation. As shown in Tab. 2, for LiDAR-based SSC models like SSCNet [55], SSCNet-full [55], LMSCNet [52], and SCPNet [65], OccFiner consistently attains relative mIoU improvements of 36.64%, 20.92%, 15.65%, and 14.83%, respectively. This demonstrates its modality-agnostic capability. We observe that the enhancements offered by OccFiner are consistent across varying distances. This improvement is not only confined to long distances and low-accuracy scenarios but also extends to challenging high-accuracy short-

Table 2: Quantitative comparison against the state-of-the-art LiDAR-based SSC methods on the SemanticKITTI validation set. † results from the official code release.

Methods	Modality	IoU (%)			mIoU (%)			Rel.
		12.8m	25.6m	51.2m	12.8m	25.6m	51.2m	
VoxFormer [27]	Camera	65.38	57.70	44.16	22.13	18.58	13.33	-
OccFiner (VoxFormer)	Camera	65.42	58.50	47.86	23.43	21.29	18.09	†24.59%
SSCNet [55]	LiDAR	50.85	52.54	44.90	17.59	17.39	14.11	-
OccFiner (SSCNet)	LiDAR	69.64	67.65	55.92	23.90	23.26	19.28	†36.64%
SSCNet-full [55]	LiDAR	64.37	61.02	50.22	20.02	19.68	16.35	-
OccFiner (SSCNet-full)	LiDAR	65.96	64.55	54.45	23.41	23.31	19.77	†20.92%
LMSCNet [52]	LiDAR	74.88	69.45	55.22	22.37	21.50	17.19	-
OccFiner (LMSC)	LiDAR	75.18	69.72	57.25	24.01	23.29	19.88	†15.65%
SCPNet† [65]	LiDAR	73.88	64.09	49.06	48.62	44.62	35.06	-
OccFiner (SCPNet)	LiDAR	76.44	67.33	57.19	48.70	45.90	40.26	†14.83%

Table 3: Semantic scene completion results on the SemanticKITTI hidden test set [2]. * represents these methods are adapted for the RGB inputs, which are implemented and reported in MonoScene [6]. † results from the official code release.

Method	Modality	 car (3.92%) bicycle (0.03%) motorcycle (0.03%) truck (0.16%) other-vehicle (0.20%) person (0.07%) bicyclist (0.07%) motorcyclist (0.05%) road (15.30%) parking (1.12%) sidewalk (1.11%) other-ground (0.56%) building (4.11%) fence (0.09%) vegetation (0.37%) trunk (0.14%) terrain (9.17%) pole (0.20%) traffic-sign (0.08%)																		IoU	mIoU
		car (3.92%)	bicycle (0.03%)	motorcycle (0.03%)	truck (0.16%)	other-vehicle (0.20%)	person (0.07%)	bicyclist (0.07%)	motorcyclist (0.05%)	road (15.30%)	parking (1.12%)	sidewalk (1.11%)	other-ground (0.56%)	building (4.11%)	fence (0.09%)	vegetation (0.37%)	trunk (0.14%)	terrain (9.17%)	pole (0.20%)		
LMSCNet* [52]	Camera	14.30	0.00	0.00	0.30	0.00	0.00	0.00	0.00	46.70	13.50	19.50	3.10	10.30	5.40	10.80	0.00	10.40	0.00	0.00	
3DSketch* [7]	Camera	17.10	0.00	0.00	0.90	0.00	0.00	0.00	0.00	37.70	0.00	19.80	0.00	12.10	3.40	10.00	0.00	16.00	0.00	0.00	
AICNet* [23]	Camera	15.30	0.00	0.00	0.70	0.00	0.00	0.00	0.00	39.30	19.80	18.30	1.60	9.60	5.00	9.60	1.90	13.50	0.10	0.00	
JS3C-Net* [70]	Camera	20.10	0.00	0.00	0.80	4.10	0.00	0.20	0.20	47.30	19.90	21.70	2.80	12.70	8.70	14.20	3.10	12.40	1.90	0.30	
OccFormer [82]	Camera	21.60	1.50	1.70	1.20	3.20	2.20	1.10	0.20	55.90	31.50	30.30	6.50	15.70	11.90	16.80	3.90	21.30	3.80	3.70	
MonoScene [6]	Camera	18.80	0.50	0.70	3.30	4.40	1.00	1.40	0.40	54.70	24.80	27.10	5.70	14.40	11.10	14.90	2.40	19.50	3.30	2.10	
TPVFormer [18]	Camera	19.20	1.00	0.50	3.70	2.30	1.10	2.40	0.30	55.10	27.40	27.20	6.50	14.80	11.00	13.90	2.60	20.40	2.90	1.50	
VoxFormer [27]	Camera	21.80	0.90	1.20	5.60	2.80	1.00	1.30	0.00	54.10	24.70	27.80	9.20	23.40	14.20	24.60	9.00	23.40	6.70	6.60	
OccFiner (Vox)	Camera	31.10	1.90	1.60	7.80	2.50	3.80	2.00	0.00	62.00	35.20	36.10	13.70	28.10	18.70	29.10	9.60	31.70	6.60	6.50	
w.r.t. VoxFormer	-	+9.30	+1.00	+0.40	+2.20	-0.30	+2.80	+0.70	-	+7.90	+10.50	+8.30	+4.50	+4.70	+4.50	+4.50	+0.60	+8.30	-0.10	-0.10	
SSCNet-Full [55]	LiDAR	24.30	0.50	0.80	1.20	4.30	0.30	0.30	0.00	51.20	27.10	30.80	6.40	34.50	19.90	35.30	18.20	29.00	13.10	6.70	
ESSCNet [50]	LiDAR	26.40	0.30	5.40	5.00	9.10	2.90	2.70	0.10	43.80	26.90	28.10	10.30	29.80	23.30	35.80	20.10	28.70	16.40	16.70	
SSCNet [52]	LiDAR	30.90	0.00	0.00	1.50	0.80	0.00	0.00	0.00	64.80	29.00	34.70	4.60	38.10	21.30	41.30	19.90	32.10	15.00	0.80	
SCPNet [65]	LiDAR	42.40	33.70	33.60	12.20	26.00	18.40	17.00	1.60	69.50	51.70	49.50	20.20	35.40	41.50	41.80	38.40	49.70	37.80	27.10	
OccFiner (SCPNet)	LiDAR	49.00	38.30	40.20	13.30	28.10	19.60	20.00	1.80	74.70	52.10	54.70	30.90	40.90	44.70	49.20	40.80	54.70	49.20	37.82	
w.r.t. SCPNet	-	+6.70	+4.60	+6.60	+1.10	+2.10	+1.20	+3.00	+0.20	+5.20	+0.40	+5.20	+1.70	+5.50	+3.20	+7.40	+2.40	+4.70	+0.60	+0.30	

range as well, indicating a robust and versatile perception of the framework. Remarkably, the accuracy of OccFiner (VoxFormer) even surpasses onboard LiDAR-based SSC models including SSCNet, SSCNet-full, and LMSCNet. This is the first time that the camera-based SSC model surpasses the LiDAR-based SSC model in accuracy. Compared with the onboard LiDAR-based LMSCNet, the camera-based OccFiner (VoxFormer) achieves a relative mIoU improvement of 5.24%. This proves that OccFiner unleashes the potential of the camera-based SSC applications. This breakthrough in the camera-based versus LiDAR-based SSC model signifies a crucial advancement for autonomous driving, notably in the realms of pure visual SSC data closure and auto-labeling.

As shown in Tab. 3, in the results submitted for the hidden test set of SemanticKITTI [2], OccFiner showcases remarkable performance. The OccFiner (Vox) and OccFiner (SCPNet) establish new state-of-the-art accuracy for camera-based and LiDAR-based SSC respectively. They deliver significant relative mIoU improvements compared to the best-published results of 26.99% and 9.50%, re-

Table 4: Benchmarking results on SSCBench-KITTI360 [26]. The default evaluation range is $51.2 \times 51.2 \times 6.4 m^3$.

Method	Input	IoU	mIoU	car	bicycle	motorcycle	truck	other-veh.	person	road	parking	sidewalk	other-grnd	building	fence	vegetation	terrain	pole	traf-sign	other-struct.	other-object
LMSNet [52]	L	47.53	13.65	20.91	0.00	0.00	0.26	0.00	0.00	62.95	13.51	33.51	0.20	43.67	0.33	40.01	26.80	0.00	0.00	3.63	0.00
SSCNet [55]	L	53.58	16.95	31.95	0.00	0.17	10.29	0.58	0.07	65.70	17.33	41.24	3.22	44.41	6.77	43.72	28.87	0.78	0.75	8.60	0.67
Voxformer [27]	C	38.76	11.91	17.84	1.16	0.89	4.56	2.06	1.63	47.01	9.67	27.21	2.89	31.18	4.97	28.99	14.69	6.51	6.92	3.79	2.43
MonoScene [6]	C	37.87	12.31	19.34	0.43	0.58	8.02	2.03	0.86	48.35	11.38	28.13	3.22	32.89	3.53	26.15	16.75	6.92	5.67	4.20	3.09
OccFiner (Mono)	C	38.51	13.29	20.78	1.08	1.03	9.04	3.58	1.46	53.47	12.55	31.27	4.13	33.75	4.62	26.83	18.67	5.04	4.58	4.05	3.32
w.r.t. MonoScene	-	<u>+0.64</u>	<u>+0.98</u>	<u>+1.44</u>	<u>+0.65</u>	<u>+0.45</u>	<u>+1.02</u>	<u>+1.55</u>	<u>+0.60</u>	<u>+5.12</u>	<u>+1.17</u>	<u>+3.14</u>	<u>+0.91</u>	<u>+0.86</u>	<u>+1.09</u>	<u>+0.68</u>	<u>+1.92</u>	<u>-1.88</u>	<u>-1.09</u>	<u>-0.15</u>	<u>-0.23</u>

Table 5: Ablation experiments. Settings used in our final framework are underlined. See Sec. 4.3 for details.

Experiment	Method	SemanticKITTI (val)			#Parameters
		Near	Middle	Far	
Reference Model (VoxFormer [27]), Training: 10 Epoch (SemanticKITTI [2]).					
Onboard Model	VoxFormer [27]	22.13	18.58	13.33	551M
DualFlow4D Transformer	w/o	21.71	19.23	13.96	+0.83M
	with	23.29	20.25	14.52	+4.51M
Temporal Embedding	Embedding	23.24	20.21	14.50	+4.90M
	Not Embedding	23.29	20.25	14.52	+4.51M
Spatial Embedding	Not Embedding	23.14	19.95	14.40	+4.12M
	Embedding	23.29	20.25	14.52	+4.51M
Reference Frame	w/o	22.99	20.04	14.30	+4.51M
	with	23.29	20.25	14.52	+4.51M
Reference Model (VoxFormer [27]), Training: 10 Epoch (SemanticKITTI [2]) → Global Prop.					
Offboard Baseline (Average Fusion)	VoxFormer [27] + Vanilla Registration	21.18	18.36	14.52	551M
	OccFiner Stage 1 + Vanilla Registration	22.60	20.19	16.11	+4.51M
Learning Refine	w/o	21.48	18.97	16.05	n.a.
	with	23.43	21.29	18.09	+4.51M
Frustum Weighting	w/o	23.09	20.80	17.63	+4.51M
	with	23.43	21.29	18.09	+4.51M
Distance-aware Weighting	w/o	23.14	20.92	17.34	+4.51M
	with	23.43	21.29	18.09	+4.51M
Temporal Input	(-5, 5)	23.41	21.11	16.25	+4.51M
	(-10, 10)	23.45	21.29	17.65	+4.51M
	(-15, 15)	23.43	21.28	18.00	+4.51M
	(-20, 20)	23.43	21.28	18.05	+4.51M
	(-25, 25)	23.43	21.29	18.09	+4.51M
	(-30, 30)	23.43	21.29	18.08	+4.51M

spectively. The OccFiner (Vox) consistently surpasses the SSCNet-full [55]. This further demonstrates the efficacy and advancement of the OccFiner framework.

The effectiveness of OccFiner is also assessed on the SSCBench-KITTI360 dataset [26]. As shown in Tab. 4, OccFiner (Mono) demonstrates notable performance, achieving a relative improvement in mIoU of 7.96% compared to MonoScene [6]. This underscores OccFiner’s capability to enhance SSC accuracy across diverse datasets.

4.3 Ablation Studies

The efficacy of each component in the offboard OccFiner framework is quantified through ablation studies detailed in Tab. 5. Using VoxFormer [27] as the onboard component, we evaluate mIoU accuracy across different distances.

Multi-to-Multi Local Propagation Network. 1) DualFlow4D Transformer. We validate the critical role of the 4D Transformer for local SSC feature propagation, evidenced by a 0.56% drop in mIoU upon its removal. 2) Temporal

Embedding, however, did not positively impact accuracy. 3) Spatial Embedding. The result highlights the importance of spatial embedding and the introduction of a long-distance reference frame in the multi-to-multi paradigm, improving accuracy by 0.12%. 4) Reference Frame. OccFiner introduces a long-distance reference frame in addition to the local clip, which further improves the accuracy by 0.22%. It proves the positive effect of long-term geometric and semantic cues on error compensation. 5) Overall, OccFiner’s first stage, while adding few model parameters (4.51M *vs.* 551M), effectively compensates for onboard model errors and propagates high-confidence features, boosting mIoU from 13.33% to 14.52%, and uniformly improves mIoU across various distances. This is critical for the next global propagation stage.

Region-centric Global Propagation. 1) Average Fusion. Average fusion applied as a baseline to the onboard model yielded only a modest mIoU improvement at ‘far’, indicating limitations at near and middle distances with 0.95% and 0.22% mIoU drop, respectively. 2) Learning Refine. Removing the local propagation network resulted in a significant drop in mIoU by 2.04%, highlighting the critical role of first-stage error compensation in enhancing global propagation accuracy across various distances. 3) Sensor Bias. the frustum weighting and distance-aware weighting adjustments are shown to be vital, with their removal leading to noticeable accuracy drops. This underscores the importance of considering the camera field of view and depth uncertainties in long-distance measurements. 4) Temporal Input. The optimal number of frames for global propagation is identified around $(-25, 25)$, with more frames offering no additional benefit. 5) Overall, learning-free global propagation significantly improves the accuracy of long-distance prediction. Compared with ‘OccFiner Stage 1 + Vanilla Registration’, OccFiner’s region-centric global propagation further improving the accuracy across different distances by 0.83%, 1.10%, and 1.98%.

5 Conclusions and Discussion

In addressing the challenges of inferior performance and data closure in vision-based SSC, we introduce OccFiner, the first offboard SSC setup to solve the unreliability of the onboard model. By removing computational constraints, OccFiner can reason all frames together and build multi-view consistent SSC predictions. Concretely, OccFiner leverages a hybrid propagation strategy. In the multi-to-multi local propagation stage, OccFiner focuses on the onboard model error compensation and implicit semantic and geometric cues propagation. In the region-centric global propagation stage, OccFiner considers sensor bias and manages long-term information aggregation. Our experimental findings validate OccFiner’s versatility across various onboard models and its capability to significantly elevate SSC quality, setting new benchmarks in vision- and LiDAR-based algorithms on SemanticKITTI. We hope that our framework can become a potent augmentor for onboard SSC algorithms and inspire future offboard research.

Limitations. Our offboard framework, OccFiner, achieves notable results but requires individual retraining for each onboard model. This process is tailored

to address the specific errors of each onboard model, with its effectiveness partly dependent on the scene’s characteristics. Additionally, there is substantial scope for improving offboard SSC accuracy in comparison to the ground truth.

Broader impact, Ethics. While OccFiner improves 3D scene understanding, potential inaccuracies in its predictions could have serious implications, especially in critical applications like autonomous driving. It is crucial that such technologies be complemented by additional safety measures to mitigate risks associated with these inevitable errors.

A Auto-labeling Experiments

Table 6: Comparison between onboard models trained with either training set ground-truth labels (GT-Train) or auto-labeling mixed GT-Train + pseudo-labels (PL) generated by different sources.

Label	Source	IoU	mIoU
GT-Train	Human Labeling	36.42	13.17
GT-Train + PL-Test (SSCNet [55])	LiDAR Auto-Labeling	37.07	13.63
GT-Train + PL-Test (VoxFormer [27])	Visual Auto-Labeling	36.15	12.74
GT-Train + PL-Test (VoxFormer [27] + OccFiner)	Visual Auto-Labeling	37.17	13.90

The main paper’s results highlight OccFiner’s ability to generate superior SSC (Semantic Scene Completion) labels, indicating its promise as an offboard solution for automatic SSC labeling and data closure, particularly for augmenting manual labeling in novel scenarios. To evaluate OccFiner’s label quality further, we conduct auto-labeling experiments on SemanticKITTI [2], detailed in Table 6, which simulate a real-world data loop. Utilizing manually annotated labels as a base, we enrich new scenes from the test sequences with pseudo-labels created by the pure-vision VoxFormer + OccFiner. Comparing training results of an onboard visual SSC model [82] *from scratch* under different labeling conditions, we find that directly using VoxFormer for ‘Visual Auto-Labeling’ cannot achieve data closure, and the IoU and mIoU of the onboard model dropped by 0.27% and 0.43%, respectively. Meanwhile, ‘LiDAR Auto-Labeling’ based on SSCNet [55] can improve the accuracy of the visual onboard model by 0.46%. Keeping hyperparameters and model structure consistent, we find that OccFiner’s ‘Visual Auto-Labeling’ outperforms ‘Human Labeling’ alone. Consequently, the onboard model’s IoU on the validation set improved by 0.75%, with a corresponding large increase of 0.73% in mIoU. When compared under varied labeling conditions, OccFiner’s visual auto-labeling significantly improves onboard model performance, demonstrating a notable advantage over both pure human labeling and even LiDAR-based auto-labeling. This underscores our method’s ability to effectively close data loops in SSC applications using high-quality, visually-derived labels.

B City-level SSC Map Comparisons

Previous works usually focus on local 3D semantic occupancy, *i.e.*, onboard perception centered on a single vehicle. However, for multi-vehicle collaborative sensing, task scheduling, and traffic control, establishing a city-level SSC map is of great significance. Therefore, we propose to fuse local SSC predictions using relative poses to further explore the effectiveness of OccFiner in establishing visually derived city-level SSC results. In the global map, we only consider static rigid targets of the scene, since dynamic targets are not among the usual properties of maps.

B.1 Quantitatively Comparisons

Table 7: City-level semantic scene completion results on the SemanticKITTI validation set [2]. Note we only compare static classes in the global map comparisons. † results from the official code release.

Method	Modality	road (15.30%)	parking (1.12%)	sidewalk (11.13%)	other-ground (0.56%)	building (14.1%)	fence (3.90%)	vegetation (39.3%)	trunk (0.51%)	terrain (9.17%)	pole (0.29%)	traffic-sign (0.08%)	IoU	mIoU
SSCNet [55]	LiDAR	32.78	11.88	18.00	0.00	14.58	9.17	26.78	13.48	26.56	19.88	4.70	30.06	16.16
SSCNet-full [55]	LiDAR	43.82	12.52	21.24	0.35	14.58	10.05	27.18	16.46	33.25	24.47	6.92	32.83	19.16
LMSCNet [52]	LiDAR	49.71	16.73	25.89	0.00	18.93	11.67	34.73	15.68	35.16	26.81	0.69	41.66	21.45
SCPNet† [65]	LiDAR	74.81	52.43	50.80	7.85	38.91	28.99	45.30	36.27	54.86	41.33	25.59	59.39	41.55
OccFiner (SCP)	LiDAR	72.76	51.56	50.57	10.03	41.40	30.61	47.09	39.86	55.11	42.64	26.76	60.16	42.58
<i>w.r.t. SCPNet</i>	-	-2.05	-0.87	-0.23	+2.18	+2.49	+1.62	+1.79	+3.59	+0.25	+1.31	+1.17	+0.77	+1.03
MonoScene [6]	Camera	47.07	10.04	15.32	0.58	10.39	9.74	17.41	5.13	25.44	7.31	5.37	29.75	13.98
OccFormer [82]	Camera	46.70	17.90	14.77	0.95	9.17	7.31	20.40	5.93	24.64	6.87	5.77	27.63	14.58
TPVFormer [18]	Camera	43.49	15.28	13.46	0.51	8.91	8.74	17.28	4.86	24.53	6.34	4.23	26.61	13.42
VoxFormer [27]	Camera	42.22	12.48	15.16	0.36	13.04	10.12	22.21	10.02	25.63	12.36	6.71	32.66	15.48
OccFiner (Vox)	Camera	47.44	16.22	21.04	0.83	13.29	9.96	27.17	10.62	24.75	10.33	5.19	33.59	16.99
<i>w.r.t. VoxFormer</i>	-	+5.22	+3.74	+5.88	+0.47	+0.25	-0.16	+4.96	+0.60	-0.88	-2.03	-1.52	+0.93	+1.51

As shown in Table 7, we benchmark the mainstream LiDAR- and camera-based SSC methods, and explore OccFiner + VoxFormer to establish an offboard city-level SSC Map. Experimental results show that the accuracy of the LiDAR-based SSC method is consistently ahead of the camera-based method in city-level SSC maps. It is worth noting that OccFiner further improves the accuracy of both LiDAR- and camera-based city-level SSC maps. Compared with the onboard component [27], the geometric IoU of OccFiner (Vox) increased by 0.93%, and the semantic mIoU improved by 1.51%. It even exceeds the LiDAR-based SSCNet-full [55] by 0.76% in geometric accuracy and surpasses the LiDAR-based SSCNet [55] by 0.83% in semantic accuracy. This once again proves that the proposed OccFiner framework can effectively unleash the potential of purely visual SSC perception solutions.

B.2 Qualitatively Comparisons

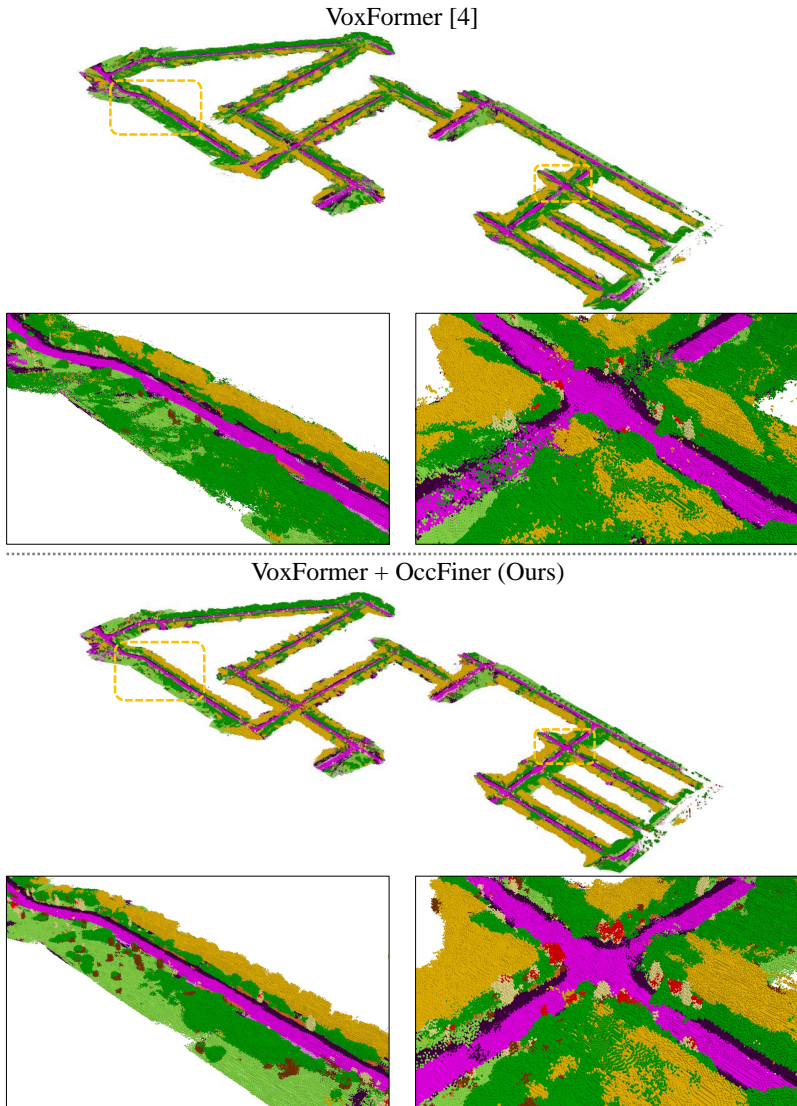


Fig. 6: City-level semantic scene completion. The city-scale scene is expanded from the original size of $256 \times 256 \times 32$ to $2205 \times 4296 \times 261$.

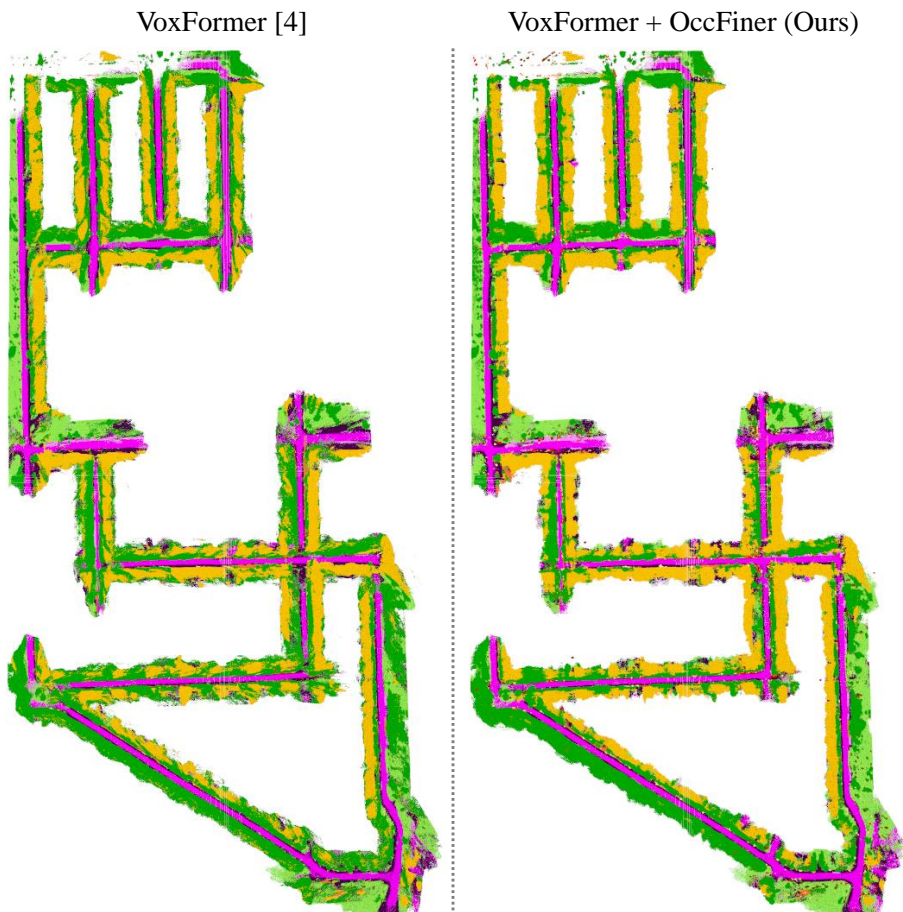
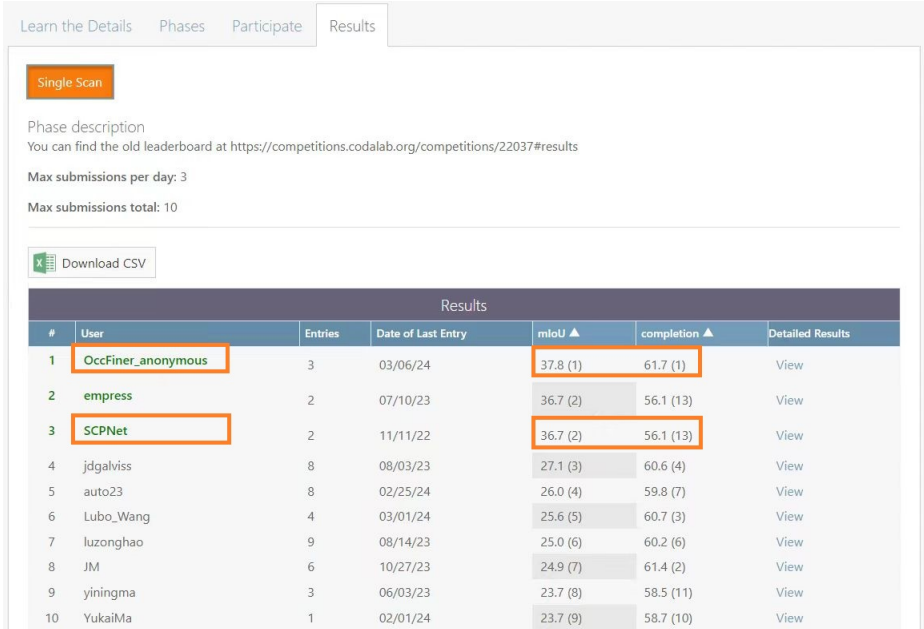


Fig. 7: City-level semantic scene completion in BEV. Only static classes are considered. Our proposed OccFiner preserves more high-quality details and reduces camera frustum artifacts.

C Screenshots of SemanticKITTI Server Results

The screenshots for SemanticKITTI [2] results on the **test server** are shown in Figure 8 and Figure 9. We have obtained the best overall results under the ‘mIoU’ and the ‘completion’ metrics. We have also obtained the best results under the pure-vision setting with a large margin over previous approaches, which signifies the effectiveness of our approach in considering the offboard problem in semantic scene completion.



#	User	Entries	Date of Last Entry	mIoU ▲	completion ▲	Detailed Results
1	OccFiner_anonymous	3	03/06/24	37.8 (1)	61.7 (1)	View
2	empress	2	07/10/23	36.7 (2)	56.1 (13)	View
3	SCPNet	2	11/11/22	36.7 (2)	56.1 (13)	View
4	jdgalviss	8	08/03/23	27.1 (3)	60.6 (4)	View
5	auto23	8	02/25/24	26.0 (4)	59.8 (7)	View
6	Lubo_Wang	4	03/01/24	25.6 (5)	60.7 (3)	View
7	luzonghao	9	08/14/23	25.0 (6)	60.2 (6)	View
8	JM	6	10/27/23	24.9 (7)	61.4 (2)	View
9	yiningma	3	06/03/23	23.7 (8)	58.5 (11)	View
10	YukaiMa	1	02/01/24	23.7 (9)	58.7 (10)	View

Fig. 8: Screenshots of SemanticKITTI [2] test results. Our proposed approach OccFiner ranks first as of March 11th, 2024.

Here are your submissions to date (✓ indicates submission on leaderboard):

#	SCORE	FILENAME	SUBMISSION DATE	SIZE (BYTES)	STATUS	✓	
1	17.2727326691	my_vox.zip	03/06/2024 10:45:27	52611	Finished		+
2	17.2727326691	OccFiner+VoxFormer.zip	03/06/2024 11:30:42	52778	Finished		+
3	37.8189431176	OccFiner+SCPNet.zip	03/06/2024 12:06:28	53075	Finished	✓	+

Fig. 9: Screenshots of SemanticKITTI [2] test server. We also rank first using the pure-vision solution, with a large margin over the previous approaches. This signifies the usefulness of considering the offboard setting in semantic scene completion.

D More Implementation Details

D.1 Multi-to-Multi Local Propagation Network Architecture

In our implementation, the BEV feature and positional encoders are structured as an embedding `Linear` layer with `LayerNorm` and four convolutional blocks. Each block uses `MaxPool` for downsampling by a factor of 2, includes two BEV 3×3 2D convolutions with `ReLU` activation, and outputs features with a channel of 80. For the DualFlow4D block’s BEV branch, we set the bev patch size at $W_h = 7$, $W_w = 7$, and $T = 6$. The local and distant reference time windows are $T_l = 4$ and $T_r = 2$, respectively, with a reference frame sampling temporal radius of $n = 10$ and a hidden dimension of $c_e = 256$. The pillar branch of the DualFlow4D block is set at $W_z = 32$ and $T = 6$. Across all experiments, we stack $N = 2$ DualFlow4D Transformer blocks to achieve the desired functionality.

D.2 Details for Region-centric Global Propagation

For global propagation in each SSC frame, we use a temporal radius of $n = 25$. Camera voting weights are set at $w_{high} = 1$, $w_{med} = 0.1$, and $w_{low} = 0.01$, with a bounding box of $25.6m \times 25.6m \times 6.4m$. For LiDAR, the voting weights range from $w_{max} = 10$ to $w_{min} = 0.1$. We employ vectorization to expedite the global propagation and, due to memory constraints, use single-precision (`float`) calculations for semantic voxel registration and 8-bit quantization (`uint8`) in generating city-level global street view maps. In addition, when determining the semantic category of each voxel of the city-level SSC map, we use a three-dimensional sliding window strategy to implement `argmax` for different map chunks and finally fuse them into a global three-dimensional semantic map to further reduce memory consumption.

E Region-Centric Global Propagation

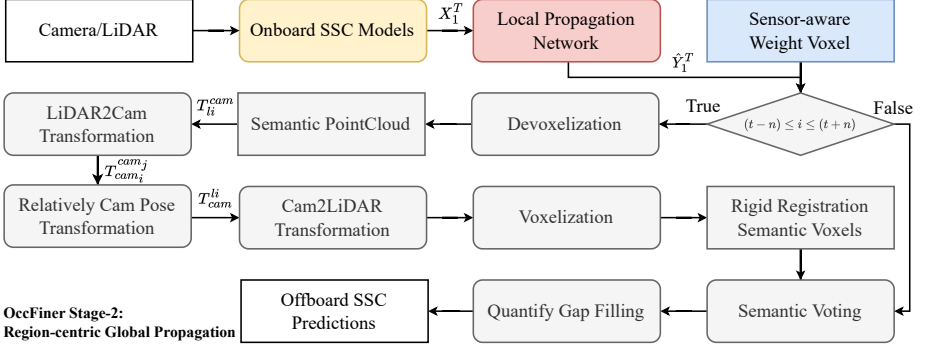


Fig. 10: Detailed pipeline of the proposed region-centric global propagation. Given an arbitrary number of input frames, we leverage multi-view geometry and consider sensor bias to augment long-term SSC consistency and accuracy.

In Figure 10, we detail the region-centric global propagation process of OccFiner’s second stage. Initially, inputs from camera or LiDAR go through the onboard component, generating preliminary predictions. The first stage involves local propagation networks applying error compensation within a brief time window. For the second phase, sensor-aware weight voxels are initialized, considering the sensor bias. Subsequently, these weight voxels and first-stage error-compensated predictions undergo devoxelization, pose transformation, and voting. The current SSC frame then refines any quantization artifacts in the transformation, culminating in the final offboard SSC predictions.

F More Visualization

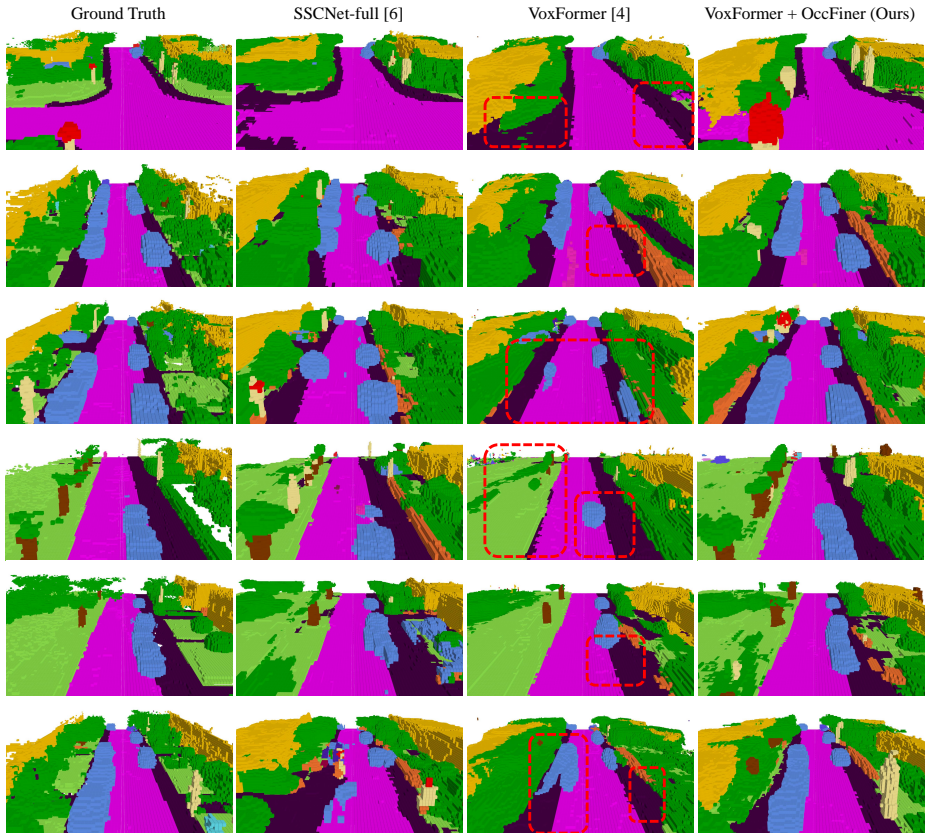


Fig. 11: More qualitative results for Semantic Scene Completion. We compare the generated results from LiDAR-based SSCNet-full [55], the vision-based VoxFormer [27], and the offboard fused results from the pure-vision VoxFormer + OccFiner. Compared with other approaches, our OccFiner achieves better fidelity for complex scene understanding.

We provide more qualitative results on semantic scene completion in Figure 11, in addition to our visualizations of the main paper. Compared with onboard approaches, our offboard OccFiner significantly improves the quality of SSC predictions for complex scene understanding.

References

1. Aygun, M., Osep, A., Weber, M., Maximov, M., Stachniss, C., Behley, J., Leal-Taixé, L.: 4D panoptic LiDAR segmentation. In: CVPR (2021) 4

2. Behley, J., Garbade, M., Milioto, A., Quenzel, J., Behnke, S., Stachniss, C., Gall, J.: SemanticKITTI: A dataset for semantic scene understanding of LiDAR sequences. In: ICCV (2019) [3](#), [10](#), [11](#), [12](#), [13](#), [15](#), [16](#), [19](#)
3. Berman, M., Triki, A.R., Blaschko, M.B.: The lovász-softmax loss: A tractable surrogate for the optimization of the intersection-over-union measure in neural networks. In: CVPR (2018) [10](#)
4. Boeder, S., Gigengack, F., Risse, B.: OccFlowNet: Towards self-supervised occupancy estimation via differentiable rendering and occupancy flow. arXiv preprint arXiv:2402.12792 (2024) [4](#)
5. Caesar, H., Bankiti, V., Lang, A.H., Vora, S., Liong, V.E., Xu, Q., Krishnan, A., Pan, Y., Baldan, G., Beijbom, O.: nuScenes: A multimodal dataset for autonomous driving. In: CVPR (2020) [4](#)
6. Cao, A.Q., de Charette, R.: MonoScene: Monocular 3D semantic scene completion. In: CVPR (2022) [1](#), [2](#), [3](#), [4](#), [10](#), [11](#), [12](#), [13](#), [16](#)
7. Chen, X., Lin, K.Y., Qian, C., Zeng, G., Li, H.: 3D sketch-aware semantic scene completion via semi-supervised structure prior. In: CVPR (2020) [11](#), [12](#)
8. Cheng, R., Agia, C., Ren, Y., Li, X., Bingbing, L.: S3CNet: A sparse semantic scene completion network for LiDAR point clouds. In: CoRL (2021) [4](#)
9. Dosovitskiy, A., Beyer, L., Kolesnikov, A., Weissenborn, D., Zhai, X., Unterthiner, T., Dehghani, M., Minderer, M., Heigold, G., Gelly, S., Uszkoreit, J., Houlsby, N.: An image is worth 16x16 words: Transformers for image recognition at scale. In: ICLR (2021) [7](#)
10. Fan, L., Yang, Y., Mao, Y., Wang, F., Chen, Y., Wang, N., Zhang, Z.: Once detected, never lost: Surpassing human performance in offline LiDAR based 3D object detection. arXiv preprint arXiv:2304.12315 (2023) [4](#)
11. Geiger, A., Lenz, P., Urtasun, R.: Are we ready for autonomous driving? The KITTI vision benchmark suite. In: CVPR (2012) [4](#)
12. Gu, S., Lu, J., Yang, J., Xu, C.Z., Kong, H.: Dense top-view semantic completion with sparse guidance and online distillation. IEEE Transactions on Intelligent Vehicles (2023) [4](#)
13. Hausman, D.M., Woodward, J.: Independence, invariance and the causal markov condition. The British Journal for the Philosophy of Science (1999) [6](#)
14. Hayler, A., Wimbauer, F., Muhle, D., Rupprecht, C., Cremers, D.: S4C: Self-supervised semantic scene completion with neural fields. arXiv preprint arXiv:2310.07522 (2023) [4](#)
15. Hong, Y., Liu, Q., Cheng, H., Ma, D., Dai, H., Wang, Y., Cao, G., Ding, Y.: UniVision: A unified framework for vision-centric 3D perception. arXiv preprint arXiv:2401.06994 (2024) [4](#)
16. Hou, J., Li, X., Guan, W., Zhang, G., Feng, D., Du, Y., Xue, X., Pu, J.: FastOcc: Accelerating 3D occupancy prediction by fusing the 2D bird's-eye view and perspective view. In: ICRA (2024) [4](#)
17. Huang, Y., Zheng, W., Zhang, B., Zhou, J., Lu, J.: SelfOcc: Self-Supervised vision-based 3D occupancy prediction. arXiv preprint arXiv:2311.12754 (2023) [4](#)
18. Huang, Y., Zheng, W., Zhang, Y., Zhou, J., Lu, J.: Tri-perspective view for vision-based 3D semantic occupancy prediction. In: CVPR (2023) [2](#), [10](#), [11](#), [12](#), [16](#)
19. Jia, Y., He, J., Chen, R., Zhao, F., Luo, H.: OccupancyDETR: Making semantic scene completion as straightforward as object detection. arXiv preprint arXiv:2309.08504 (2023) [4](#)
20. Jiang, H., Cheng, T., Gao, N., Zhang, H., Liu, W., Wang, X.: Symphonize 3D semantic scene completion with contextual instance queries. In: CVPR (2024) [4](#)

21. Kingma, D.P., Ba, J.: Adam: A method for stochastic optimization. In: ICLR (2015) [10](#)
22. Li, B., Sun, Y., Liang, Z., Du, D., Zhang, Z., Wang, X., Wang, Y., Jin, X., Zeng, W.: Bridging stereo geometry and BEV representation with reliable mutual interaction for semantic scene completion. arXiv preprint arXiv:2303.13959 (2023) [4](#)
23. Li, J., Han, K., Wang, P., Liu, Y., Yuan, X.: Anisotropic convolutional networks for 3D semantic scene completion. In: CVPR (2020) [11](#), [12](#)
24. Li, L., Shao, W., Dong, W., Tian, Y., Yang, K., Zhang, W.: Data-centric evolution in autonomous driving: A comprehensive survey of big data system, data mining, and closed-loop technologies. arXiv preprint arXiv:2401.12888 (2024) [2](#)
25. Li, X., Wang, Z., Huang, Y., Chen, H.: A survey on self-evolving autonomous driving: A perspective on data closed-loop technology. IEEE Transactions on Intelligent Vehicles (2023) [2](#)
26. Li, Y., Li, S., Liu, X., Gong, M., Li, K., Chen, N., Wang, Z., Li, Z., Jiang, T., Yu, F., Wang, Y., Zhao, H., Yu, Z., Feng, C.: SSCBench: A large-scale 3D semantic scene completion benchmark for autonomous driving. arXiv preprint arXiv:2306.09001 (2023) [4](#), [10](#), [13](#)
27. Li, Y., Yu, Z., Choy, C., Xiao, C., Alvarez, J.M., Fidler, S., Feng, C., Anandkumar, A.: VoxFormer: Sparse voxel transformer for camera-based 3D semantic scene completion. In: CVPR (2023) [1](#), [2](#), [3](#), [10](#), [11](#), [12](#), [13](#), [15](#), [16](#), [22](#)
28. Li, Y., Zhang, J., Ma, D., Wang, Y., Feng, C.: Multi-robot scene completion: Towards task-agnostic collaborative perception. In: CoRL (2023) [4](#)
29. Li, Z., Yu, Z., Austin, D., Fang, M., Lan, S., Kautz, J., Alvarez, J.M.: FB-OCC: 3D occupancy prediction based on forward-backward view transformation. arXiv preprint arXiv:2307.01492 (2023) [4](#)
30. Liao, Y., Xie, J., Geiger, A.: KITTI-360: A novel dataset and benchmarks for urban scene understanding in 2D and 3D. IEEE Transactions on Pattern Analysis and Machine Intelligence (2023) [10](#)
31. Liu, H., Wang, H., Chen, Y., Yang, Z., Zeng, J., Chen, L., Wang, L.: Fully sparse 3D panoptic occupancy prediction. arXiv preprint arXiv:2312.17118 (2023) [4](#)
32. Lu, J., Gu, S., Xu, C.Z., Kong, H.: A cylindrical convolution network for dense top-view semantic segmentation with LiDAR point clouds. In: ACCV (2022) [4](#)
33. Lu, Y., Zhu, X., Wang, T., Ma, Y.: OctreeOcc: Efficient and multi-granularity occupancy prediction using octree queries. arXiv preprint arXiv:2312.03774 (2023) [4](#)
34. Lyu, C., Guo, S., Zhou, B., Xiong, H., Zhou, H.: 3DOPFormer: 3D occupancy perception from multi-camera images with directional and distance enhancement. IEEE Transactions on Intelligent Vehicles (2023) [4](#)
35. Ma, J., Chen, X., Huang, J., Xu, J., Luo, Z., Xu, J., Gu, W., Ai, R., Wang, H.: Cam4DOcc: Benchmark for camera-only 4D occupancy forecasting in autonomous driving applications. In: CVPR (2024) [4](#)
36. Ma, Q., Tan, X., Qu, Y., Ma, L., Zhang, Z., Xie, Y.: COTR: Compact occupancy transformer for vision-based 3D occupancy prediction. arXiv preprint arXiv:2312.01919 (2023) [4](#)
37. Ma, T., Yang, X., Zhou, H., Li, X., Shi, B., Liu, J., Yang, Y., Liu, Z., He, L., Qiao, Y., Li, Y., Li, H.: DetZero: Rethinking offboard 3D object detection with long-term sequential point clouds. In: ICCV (2023) [4](#)
38. Mei, J., Yang, Y., Wang, M., Zhu, J., Zhao, X., Ra, J., Li, L., Liu, Y.: Camera-based 3D semantic scene completion with sparse guidance network. arXiv preprint arXiv:2312.05752 (2023) [4](#)

39. Miao, R., Liu, W., Chen, M., Gong, Z., Xu, W., Hu, C., Zhou, S.: OcDepth: A depth-aware method for 3D semantic scene completion. arXiv preprint arXiv:2302.13540 (2023) [4](#)
40. Min, C., Xiao, L., Zhao, D., Nie, Y., Dai, B.: Occupancy-MAE: Self-supervised pre-training large-scale LiDAR point clouds with masked occupancy autoencoders. IEEE Transactions on Intelligent Vehicles (2023) [4](#)
41. Min, C., Xiao, L., Zhao, D., Nie, Y., Dai, B.: Multi-camera unified pre-training via 3D scene reconstruction. IEEE Robotics and Automation Letters (2024) [4](#)
42. Ming, Z., Berrio, J.S., Shan, M., Worrall, S.: InverseMatrixVT3D: An efficient projection matrix-based approach for 3D occupancy prediction. arXiv preprint arXiv:2401.12422 (2024) [4](#)
43. Ming, Z., Berrio, J.S., Shan, M., Worrall, S.: OccFusion: A straightforward and effective multi-sensor fusion framework for 3D occupancy prediction. arXiv preprint arXiv:2403.01644 (2024) [4](#)
44. Najibi, M., Ji, J., Zhou, Y., Qi, C.R., Yan, X., Ettinger, S., Anguelov, D.: Motion inspired unsupervised perception and prediction in autonomous driving. In: ECCV (2022) [4](#)
45. Pan, M., Liu, J., Zhang, R., Huang, P., Li, X., Liu, L., Zhang, S.: RenderOcc: Vision-centric 3D occupancy prediction with 2D rendering supervision. arXiv preprint arXiv:2309.09502 (2023) [4](#)
46. Pang, Z., Li, Z., Wang, N.: Model-free vehicle tracking and state estimation in point cloud sequences. In: IROS (2021) [4](#)
47. Park, J., Xu, C., Yang, S., Keutzer, K., Kitani, K., Tomizuka, M., Zhan, W.: Time will tell: New outlooks and a baseline for temporal multi-view 3D object detection. In: ICLR (2022) [4](#)
48. Peng, K., Fei, J., Yang, K., Roitberg, A., Zhang, J., Bieder, F., Heidenreich, P., Stiller, C., Stiefelhagen, R.: MASS: Multi-attentional semantic segmentation of LiDAR data for dense top-view understanding. IEEE Transactions on Intelligent Transportation Systems (2022) [4](#)
49. Peng, L., Xu, J., Cheng, H., Yang, Z., Wu, X., Qian, W., Wang, W., Wu, B., Cai, D.: Learning occupancy for monocular 3D object detection. arXiv preprint arXiv:2305.15694 (2023) [4](#)
50. Qi, C.R., Zhou, Y., Najibi, M., Sun, P., Vo, K., Deng, B., Anguelov, D.: Offboard 3D object detection from point cloud sequences. In: CVPR (2021) [4](#)
51. Rist, C.B., Emmerichs, D., Enzweiler, M., Gavrila, D.M.: Semantic scene completion using local deep implicit functions on LiDAR data. IEEE Transactions on Pattern Analysis and Machine Intelligence (2022) [4](#)
52. Roldao, L., de Charette, R., Verroust-Blondet, A.: LMSCNet: Lightweight multi-scale 3D semantic completion. In: 3DV (2020) [1](#), [3](#), [4](#), [11](#), [12](#), [13](#), [16](#)
53. Silva, S., Wannigama, S.B., Ragel, R., Jayatilaka, G.: S2TPVFormer: Spatio-temporal tri-perspective view for temporally coherent 3D semantic occupancy prediction. arXiv preprint arXiv:2401.13785 (2024) [4](#)
54. Song, R., Liang, C., Cao, H., Yan, Z., Zimmer, W., Gross, M., Festag, A., Knoll, A.: Collaborative semantic occupancy prediction with hybrid feature fusion in connected automated vehicles. In: CVPR (2024) [4](#)
55. Song, S., Yu, F., Zeng, A., Chang, A.X., Savva, M., Funkhouser, T.: Semantic scene completion from a single depth image. In: CVPR (2017) [3](#), [11](#), [12](#), [13](#), [15](#), [16](#), [22](#)
56. Sun, P., Kretschmar, H., Dotiwalla, X., Chouard, A., Patnaik, V., Tsui, P., Guo, J., Zhou, Y., Chai, Y., Caine, B., Vasudevan, V., Han, W., Ngiam, J., Zhao, H., Timofeev, A., Ettinger, S., Krivokon, M., Gao, A., Joshi, A., Zhang, Y., Shlens, J.,

- Chen, Z., Anguelov, D.: Scalability in perception for autonomous driving: Waymo open dataset. In: CVPR (2020) 4
57. Tan, Z., Dong, Z., Zhang, C., Zhang, W., Ji, H., Li, H.: OVO: Open-vocabulary occupancy. arXiv preprint arXiv:2305.16133 (2023) 4
 58. Tian, X., Jiang, T., Yun, L., Wang, Y., Wang, Y., Zhao, H.: Occ3D: A large-scale 3D occupancy prediction benchmark for autonomous driving. In: NeurIPS (2023) 4
 59. Tong, W., Sima, C., Wang, T., Chen, L., Wu, S., Deng, H., Gu, Y., Lu, L., Luo, P., Lin, D., Li, H.: Scene as occupancy. In: ICCV (2023) 4
 60. Vobecky, A., Siméoni, O., Hurych, D., Gidaris, S., Bursuc, A., Pérez, P., Sivic, J.: POP-3D: Open-vocabulary 3D occupancy prediction from images. In: NeurIPS (2023) 4
 61. Wang, S., Zhu, J., Zhang, R.: Meta-RangeSeg: LiDAR sequence semantic segmentation using multiple feature aggregation. IEEE Robotics and Automation Letters (2022) 4
 62. Wang, X., Zhu, Z., Xu, W., Zhang, Y., Wei, Y., Chi, X., Ye, Y., Du, D., Lu, J., Wang, X.: OpenOccupancy: A large scale benchmark for surrounding semantic occupancy perception. In: ICCV (2023) 4
 63. Wang, Y., Chen, Y., Liao, X., Fan, L., Zhang, Z.: PanoOcc: Unified occupancy representation for camera-based 3D panoptic segmentation. arXiv preprint arXiv:2306.10013 (2023) 4
 64. Wei, Y., Zhao, L., Zheng, W., Zhu, Z., Zhou, J., Lu, J.: SurroundOcc: Multi-camera 3D occupancy prediction for autonomous driving. In: ICCV (2023) 4
 65. Xia, Z., Liu, Y., Li, X., Zhu, X., Ma, Y., Li, Y., Hou, Y., Qiao, Y.: SCPNet: Semantic scene completion on point cloud. In: CVPR (2023) 3, 4, 11, 12, 16
 66. Xiao, H., Xu, H., Kang, W., Li, Y.: Instance-aware monocular 3D semantic scene completion. IEEE Transactions on Intelligent Transportation Systems (2024) 4
 67. Xie, Z., Pang, Z., Wang, Y.X.: MV-Map: Offboard HD map generation with multi-view consistency. In: ICCV (2023) 4
 68. Xu, J., Peng, L., Cheng, H., Xia, L., Zhou, Q., Deng, D., Qian, W., Wang, W., Cai, D.: Regulating intermediate 3D features for vision-centric autonomous driving. In: AAAI (2024) 4
 69. Yan, X., Chen, R., Zhang, B., Yuan, J., Cai, X., Shi, B., Shao, W., Yan, J., Luo, P., Qiao, Y.: SPOT: Scalable 3D pre-training via occupancy prediction for autonomous driving. arXiv preprint arXiv:2309.10527 (2023) 4
 70. Yan, X., Gao, J., Li, J., Zhang, R., Li, Z., Huang, R., Cui, S.: Sparse single sweep LiDAR point cloud segmentation via learning contextual shape priors from scene completion. In: AAAI (2021) 4, 11, 12
 71. Yang, B., Bai, M., Liang, M., Zeng, W., Urtasun, R.: Auto4D: Learning to label 4D objects from sequential point clouds. arXiv preprint arXiv:2101.06586 (2021) 4
 72. Yang, J., Li, C., Zhang, P., Dai, X., Xiao, B., Yuan, L., Gao, J.: Focal attention for long-range interactions in vision transformers. In: NeurIPS (2021) 7
 73. Yang, X., Zou, H., Kong, X., Huang, T., Liu, Y., Li, W., Wen, F., Zhang, H.: Semantic segmentation-assisted scene completion for LiDAR point clouds. In: IROS (2021) 4
 74. Yao, J., Zhang, J.: DepthSSC: Depth-spatial alignment and dynamic voxel resolution for monocular 3D semantic scene completion. arXiv preprint arXiv:2311.17084 (2023) 4

75. Yu, Z., Shu, C., Deng, J., Lu, K., Liu, Z., Yu, J., Yang, D., Li, H., Chen, Y.: FlashOcc: Fast and memory-efficient occupancy prediction via channel-to-height plugin. arXiv preprint arXiv:2311.12058 (2023) [4](#)
76. Yuan, L., Chen, Y., Wang, T., Yu, W., Shi, Y., Jiang, Z., Tay, F.E., Feng, J., Yan, S.: Tokens-to-token ViT: Training vision transformers from scratch on ImageNet. In: ICCV (2021) [7](#)
77. Zhang, C., Guo, R., Zeng, W., Xiong, Y., Dai, B., Hu, R., Ren, M., Urtasun, R.: Rethinking closed-loop training for autonomous driving. In: ECCV (2022) [2](#)
78. Zhang, C., Yan, J., Wei, Y., Li, J., Liu, L., Tang, Y., Duan, Y., Lu, J.: OccNeRF: Self-supervised multi-camera occupancy prediction with neural radiance fields. arXiv preprint arXiv:2312.09243 (2023) [4](#)
79. Zhang, H., Yan, X., Bai, D., Gao, J., Wang, P., Liu, B., Cui, S., Li, Z.: RadOcc: Learning cross-modality occupancy knowledge through rendering assisted distillation. In: AAAI (2024) [4](#)
80. Zhang, J., Zhao, H., Yao, A., Chen, Y., Zhang, L., Liao, H.: Efficient semantic scene completion network with spatial group convolution. In: ECCV (2018) [12](#)
81. Zhang, Y., Li, J., Luo, K., Yang, Y., Han, J., Liu, N., Qin, D., Han, P., Xu, C.: V2VSSC: A 3D semantic scene completion benchmark for perception with vehicle to vehicle communication. arXiv preprint arXiv:2402.04671 (2024) [4](#)
82. Zhang, Y., Zhu, Z., Du, D.: OccFormer: Dual-path transformer for vision-based 3D semantic occupancy prediction. arXiv preprint arXiv:2304.05316 (2023) [4](#), [11](#), [12](#), [15](#), [16](#)
83. Zheng, W., Chen, W., Huang, Y., Zhang, B., Duan, Y., Lu, J.: OccWorld: Learning a 3D occupancy world model for autonomous driving. arXiv preprint arXiv:2311.16038 (2023) [4](#)
84. Zhou, Q., Cao, J., Leng, H., Yin, Y., Kun, Y., Zimmermann, R.: SOGDet: Semantic-occupancy guided multi-view 3D object detection. In: AAAI (2024) [4](#)
85. Zuo, S., Zheng, W., Huang, Y., Zhou, J., Lu, J.: PointOcc: Cylindrical tri-perspective view for point-based 3D semantic occupancy prediction. arXiv preprint arXiv:2308.16896 (2023) [4](#)